Printed ISSN 1330–0016
Online ISSN 1333–9133
CD ISSN 1333–8390
CODEN FIZBE7

HIGH-RESOLUTION Λ HYPERNUCLEAR SPECTROSCOPY BY THE (e,e'K$^+$) REACTION

TOMISLAV ŠEVA for the E01-011 Collaboration

Department of Physics, University of Zagreb, Bijenička 32,10000 Zagreb, Croatia

Received 20 December 2010; Revised manuscript received 28 October 2011
Accepted 7 December 2011 Online 30 December 2011

The E01-011 (HKS) experiment is the second-generation hypernuclear spectroscopy experiment by the (e,e'K$^+$) reaction at the Thomas Jefferson National Accelerator Facility (JLab). This is the continuation of the hypernuclear physics program at JLab Hall C established by the E89-009 (HNSS) experiment which demonstrated feasibility of electroproduction of hypernuclei with sub-MeV resolution. The immediate goal of the HKS experiment is to study hypernuclei in the medium-heavy region. To achieve this goal, the new high-resolution kaon spectrometer (HKS) was constructed and built, and new method in tagging the scattered electrons, the so called Tilt method, was implemented. Preliminary high-resolution spectra of ${}^{7}_{\Lambda}$He, ${}^{12}_{\Lambda}$B and ${}^{28}_{\Lambda}$Al hypernuclei are presented and discussed.

PACS number: 21.80+a UDC 539.172

Keywords: strangeness, hypernuclei, electroproduction, spectroscopy, high precision, high resolution, charge symmetry breaking

1. *Introduction*

A hypernucleus is a particle-stable nuclear system formed when one or more nucleons in a normal nucleus are replaced by strange baryons - the hyperons. With this new degree of freedom, the strangeness, hyperon is distinguishable from nucleons and therefore does not experience Pauli blocking from nucleons in the nucleus. As a result hyperon can populate deeply-bound states. By studying this type of nuclear systems, both experimentally and theoretically, deeper understanding of the baryon-baryon interaction will be gained in terms of the ΛN interaction, nuclear structure and it's features.

Hypernucleus can be produced with all interactions that produce hyperons in the nucleus [1, 2], but experimentally useful [3] are only those with significant cross section and detectable reaction products. Experimental effort has been focused on the study of Λ-hypernuclei mostly with secondary meson (K,π) beams through

(K^-, π^-) [4–11] and (π^+, K^+) [12–16] reaction. Recently two new techniques have been developed: the high resolution (a few kev) gamma spectroscopy [17–20] and electroproduction of strangeness through $(e, e'K^+)$ reaction [21,22].

1.1. Electroproduction of strangeness

The basic characteristics of photoproduction interactions (γ, K^+), with real $(\gamma + p \to K^+ + \Lambda)$ and virtual photons $(e + p \to e' + K^+ + \Lambda/\Sigma^0)$ (see Fig. 1), are large momentum transfer ($q > 300$ MeV) to the created hyperon and the strong spin-flip ($\triangle S = 1$) terms [23–26]. The spin-flip, due to the virtual photon γ^* spin, means that photoproduction reactions will excite states with natural and unnatural parity. The spin-flip unnatural parity states with $J = J_{max} = l_n + l_\Lambda + 1$ are suppressed in (K^-, π^-) and (π^+, K^+) reactions. Thus photoproduction reaction produces complementary states to those produced by hadronic reactions.

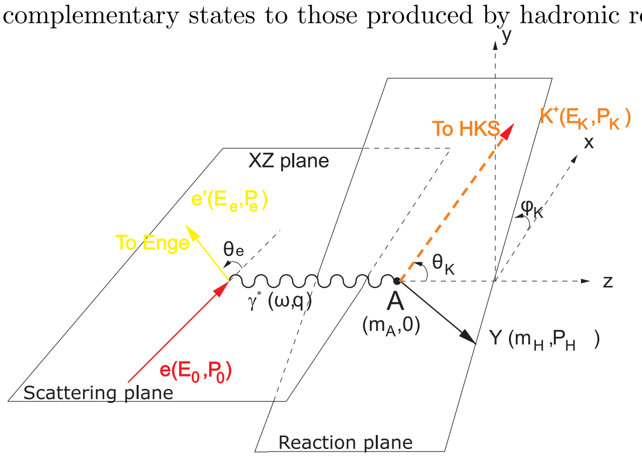

Fig. 1. Electroproduction of hypernuclei by $(e, e^{'}K^+)$ *reaction.*

The disadvantage of the photoproduction is the small cross section. On the other hand, in contrast to the purely hadronic processes, target nuclei are essentially transparent to the incident photons and the distortion of K^+ is rather small. Due to transparency of the nuclei to the incident photons, deeply bound particle-hole states can be formed with Λ deep inside nuclei for heavy nuclei. Additionally, since $(e, e'K^+)$ reaction uses low emittance and high energy stability ($< 10^{-4}$) primary electron beam, the beam energy uncertainty is very small. With well defined beam energy, high beam intensity and high resolution spectrometers, hypernuclear states can be observed with sub-MeV resolution which may allow us to observe the spin-orbit splittings for high orbital states.

In contrast to the hadronic processes, which produce hyperons in interaction with neutrons, in the electroproduction $(e, e'K^+)$ interaction hyperons are created on protons and so, for zero isospin $T = 0$ nuclei, it will produce neutron rich $T > 0$ mirror hypernucleus to those from (K^-, π^-) and (π^+, K^+) reactions. By studying the mirror hypernuclei, created by $(e, e'K^+)$ and (K^-, π^-) or (π^+, K^+)

reactions, Charge symmetry breaking effect (CSB), expected to be significant for heavy hypernuclei with large neutron excess, can be studied.

2. Experimental setup

To fully exploit electromagnetic probes in the production of hypernuclei, experimental setup of HKS experiment was designed to (1) improve the energy resolution (especially for the outgoing kaons), (2) increase the hypernuclear production yield and (3) significantly reduce the accidental background. To achieve this, new experimental technique and major equipment upgrades [27] were made from the HNSS experiment, first ever to use the $(e, e'K^+)$ reaction for production of hypernuclei [21, 22].

2.1. Experiment kinematics

Basic kinematics of the $\left(e, e^{'} K^+\right)$ reaction, as used in the Hall C HKS experiment, is illustrated in Fig. 1. Incident electron with energy of 1.854 GeV, through the emission of a virtual photon, interacts with the proton embedded in a nucleus. Scattered electron reaches the electron spectrometer (ENGE) scattering plane with central momentum of 0.319 GeV/c, which means that virtual photon carries momentum of $\approx$ 1.5 GeV. Virtual photon interacts with proton and creates strange quark-antiquark pair, and as a result the proton is converted into one strange hadron, Λ with quark content uds, and one strange meson, kaon K^+ with quark content $u\bar{s}$. Λ remains in the nucleus forming a bound state with binding energy E$_b$, and kaon K^+ is emitted with central momentum of 1.2 GeV/c.

Beam energy value was set to optimize virtual photon flux and avoid opening of other channels for kaon production. Choice of scattered electron central momentum allowed the use of existing electron spectrometer (ENGE, used in the pioneering HNSS experiment) and limited contribution of electron momentum to resolution. Virtual photon energy was set in the region where the total cross section for kaon photoproduction channel $p\,(\gamma, K^+)\,\Lambda$ is maximal, as seen in Fig. 2 [28, 29, 23]. Kaon kinematics ensured good survival rate of K$^+$ and with the newly designed spectrometer a good momentum resolution.

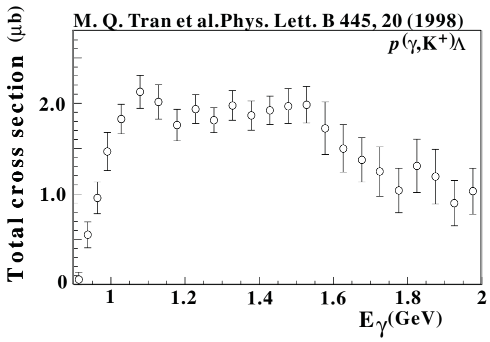

Fig. 2. Total cross section of the $p(\gamma, K^+)\Lambda$ reaction [28].

Momentum vectors at the target of scattered electron and kaon are reconstructed from focal plane variables (angles and position) by backward matrices. With known initial particle momentum vectors, hypernuclear missing mass (MM_{HY}) can be calculated with the following equation:

$$\begin{aligned} MM_{HY} &= \sqrt{E_{HY}^2 - \boldsymbol{P}_{HY}^2} \\ &= \sqrt{(E_0 + M_A - E_e - E_{K^+})^2 - (\boldsymbol{P}_0 - \boldsymbol{P}_e - \boldsymbol{P}_{K^+})^2} \end{aligned} \tag{1}$$

where M_A represents mass of the target nucleus; E_0, E_e and E_{K^+} are energies of incident electron (electron beam), scattered electron and K^+, respectively; P_0, P_e and P_{K^+} are momentum vectors of incident electron, scattered electron and kaon, respectively, as shown in Fig. 1.

2.2. Experimental apparatus

Configuration of the E01-011 experiment is shown in Fig. 3 [27]. There are two crucial experimental points in electroproduction of strangeness: (1) high quality, high intensity electron beam and (2) spectrometer system designed to ensure hypernuclear resolution and yields to compensate for the small cross section of the electroproduction.

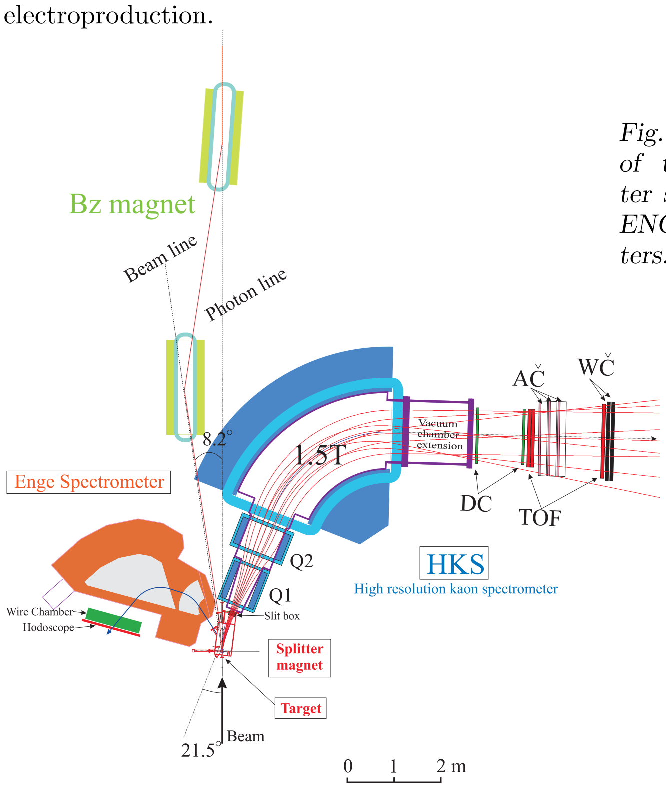

Fig. 3. Schematic overview of the E01-011 spectrometer system: Splitter magnet, ENGE and HKS spectrometers.

Requirements on electron beam are GeV energy, high resolution and intensity and 100% duty factor since it is necessary to detect a kaon and a scattered electron in coincidence. Only CEBAF (Continuous Electron Beam Accelerator Facility) at JLab meets these requirements.

2.2.1. Spectrometer system

Spectrometer system consists of the splitter magnet, high resolution kaon spectrometer (HKS) and electron spectrometer (ENGE). ENGE was used in the new configuration, the so called Tilt method, as discussed below. The splitter magnet is installed immediately downstream of the target to deflect scattered electrons and positive kaons at very forward angles to respective spectrometers. With the splitter magnet it is possible to detect electroproduced kaon and scattered electron at very forward angles where the hypernuclear cross section by the electroproduction proccess is maximal and by that to maximize the hypernuclear yield, see Fig. 5. At the same time, with the splitter, positive and negative charged particles are separated and guided to respective spectrometers and detector systems. It is worth pointing out, that thanks to the large momentum acceptance of both the kaon and scattered electron spectrometers with E01-011 setup, elementary production processes $p(e,e'K^+)\Lambda)$ and $p(e,e'K^+)\Sigma)$ and wide region of hypernuclei can be studied. These elementary processes are used for the definition of absolute mass and are a crucial part of the optics calibration.

High resolution kaon spectrometer (HKS) system was specifically built for the purpose of hypernuclear physics at JLab. The HKS consists of two quadrupoles, one vertically (Q2) and one horizontally (Q1) focusing, followed by a horizontally bending dipole. Compared to the SOS spectrometer, used in the HNSS experiment, HKS has three times larger solid angle of acceptance (≈ 15 msr) and a momentum resolution as good as 2×10^{-4}.

Tilt method stands for the simultaneous usage of vertical offsets and tilt of the ENGE spectrometer with respect to the splitter dispersion plane, as shown in Fig. 4.

Fig. 4. ENGE configuration as used in E89-009: ENGE set in the Splitter plane, and for E01-001: ENGE had vertical offset and tilt with respect to the Splitter plane.

This reduced huge background caused by the high rates of bremsstrahlung and Møller scattered electrons, as seen in the HNSS experiment. Reduction of electromagnetic background is crucial, especially in high-mass targets, since background rates are proportional to Z^2. Tilt method uses the fact that angular distributions of bremsstrahlung electrons, Møller electrons and electrons related to virtual photon are different (and beam energy dependent), as seen in Fig. 5. Angular distributions of bremsstrahlung electrons and Møller electrons depend on the beam energy, peaking more forwardly with higher beam energy, with Møller electrons extending to larger angles. By setting the acceptance of the electron spectrometer to block electrons from near zero degrees up to outside of the Møller ring the background electron rate decreased by a factor of $\approx 10^4$. The reduction of the tagged virtual photon flux rate was less severe and was compensated with high luminosity of the electron beam. The optimal tilt angle for the E01-011 experiment was found to be 7.75 degrees. This configuration allowed strangeness production on 100 mg/cm^2 ^{12}C target with electron beam of 30 μA with a higher physics yield, while maintaining a background electron rate 100 times lower than that of HNSS, even though the luminosity was more than 150 times brighter.

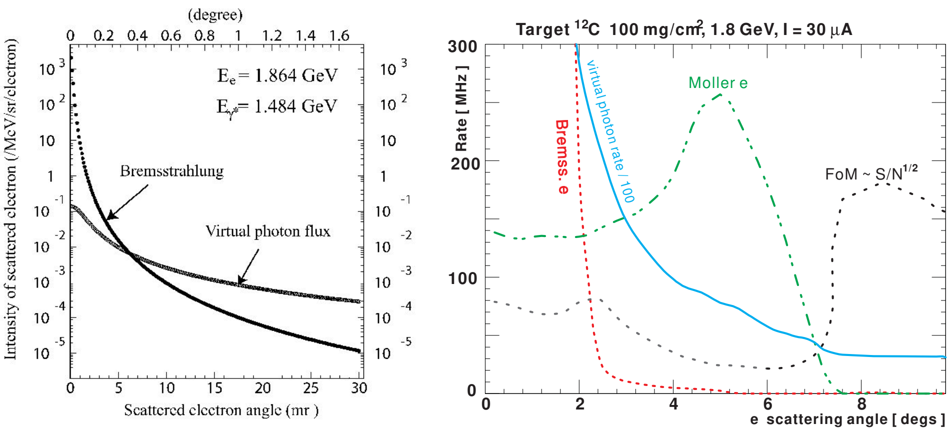

Fig. 5. Angular dependence of the calculated rates for bremsstrahlung and Møller scattered electrons and virtual photo flux. Rates are calculated for ^{12}C *target with density 100* mg/cm^2 *at beam current I=30μ*A. *Figure of merit (FoM) defined as FoM=* $S/A^{\frac{1}{2}}$*, S- virtual photon flux; A - sum of bremsstrahlung and Møller scattered electrons, FoM is scaled with arbitrary factor [27].*

2.2.2. **Detector package**

The electron arm detector package consisted of two layers of hodoscopes and honeycomb drift chamber (EDC). Hodoscopes provided timing information of scattered electrons and EDC was used to reconstruct their trajectories.

Key component of the kaon arm detector package was particle identification package (PID) needed to suppress high rates of protons and pions on trigger level and kaon event selection in analysis. Because E01-011 ran with much higher luminosity than E89-009, proton and pion rates in present study were much higher. In the E01-011 setup, PID system consisted of Water and Aerogel Čerenkov counter arrays and time of flight hodoscopes. In analysis, information from time of flight hodoscopes was used to calculate particle β, another good PID tool. Three layers of Aerogel Čerenkov counters ($n = 1.05$) were installed to ensure suppression of pions in trigger of the order of 10^{-3}. Two layers of water Čerenkov counter arrays with wave length shifter ($n = 1.33$) were installed to reject protons. PID system was placed behind the two sets of drift chambers and was used to determine kaon trajectory described by the set of focal plane angels and position. Effect of Aerogel and Water Čerenkov PID in selection of kaons in β_{ToF} spectrum is shown in Fig. 6.

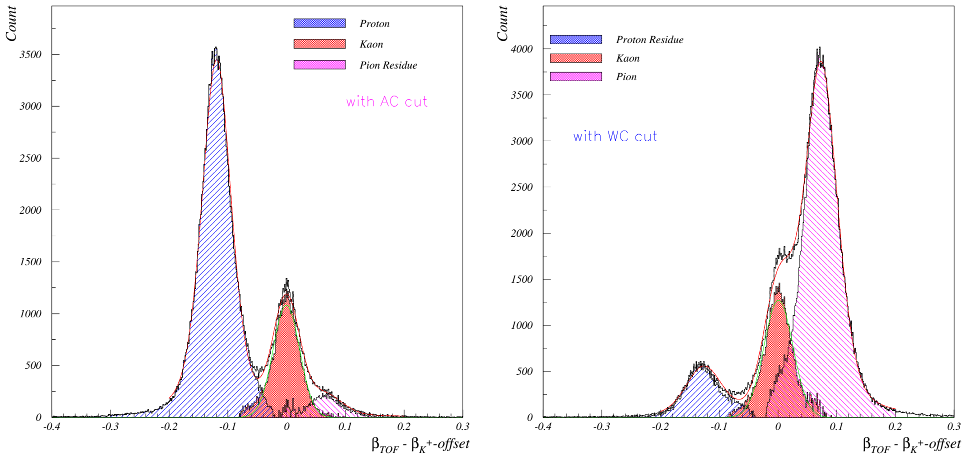

Fig. 6. β_{ToF} spectrum with applied Aerogel Čerenkov cut (Left) and Water Čerenkov cut (Right)

3. Preliminary results

Effectiveness of the experimental setup. To fully use the capabilities and unique characteristics of the $(e, e'K^+)$ reaction for the hypernuclear spectroscopy, especially for heavier systems, high background flux of bremsstrahlung electrons that limited hypernuclear yields in the HNSS experiment had to be reduced. To achieve this for the HKS experiment, new electron arm configuration, the so called "Tilt method" was introduced. The expected benefits are smaller rates of scattered electrons in the ENGE spectrometer as a result of suppression of flux of bremsstrahlung and Møller scattered electrons. This leads to a better signal to accidental (S/A) ratio and higher hypernuclear production rates. As a result heavier targets with higher on target beam currents can be studied.

The effect of the E01-011 experimental configuration and the comparison of the performance of E89-009 and E01-011 [30–31] experiments is discussed here. Information for the HNSS experiment was taken from Refs. [21], [33] and [34].

Results from the E01-011 data from CH_2 target, when compared to E89-009, showed improvement in the number of Λ counts above accidental background and ^{12}C quasi-free and better S/A ratio in coincidence time distribution. From the CH_2 data taken in roughly 84 hours, there are ≈ 2700 counts in Λ peak, compared to ≈ 210 counts from 170 hours of data taking obtained in the E89-009 experiment. Figure 7 shows comparison of coincidence time distributions and a clear improvement with ≈ 2.5 better S/A ratio in the E01-011 data. Figure 8 shows comparison of missing mass spectra with E01-011 having higher statistics and ≈ 6 times better signal to accidental background ratio.

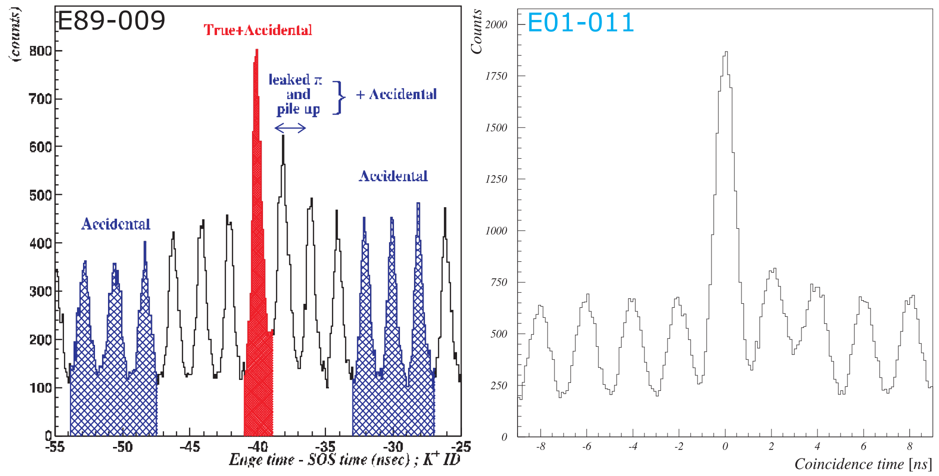

Fig. 7. Comparison between E89-099 and E01-011 coincidence time distributions. Data from CH_2 *target with imposed* K^+ *PID.*

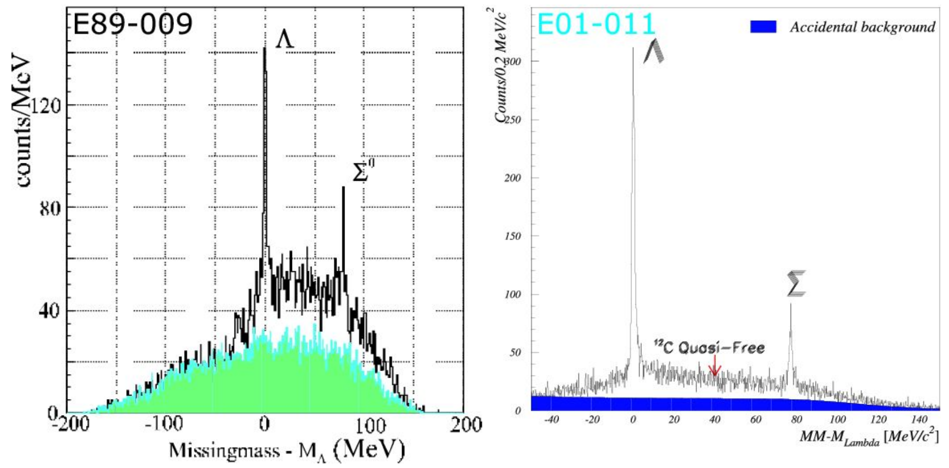

Fig. 8. Comparison between E89-099 and E01-011 missing mass spectra from CH_2 *target.*

The comparison of key performance factors between E089-009 [21] [22] and E01-011 experiment are summarized in Table 1. Missing-mass spectra of the ${}^{12}_{\Lambda}$B hypernucleus with overlayed accidental background are compared in Fig. 9. The number of counts in the ${}^{12}_{\Lambda}$B ground state doublet above accidental background for 200 hours of the E01-011 data taking is estimated to be ≈ 620 compared to ≈ 165 counts for 440 hours in the E89-009 experiment.

From the information listed in Table 1 and Figures 7, 8 and 9 the conclusion is that experimental configuration of the E01-011 experiment with implemented HKS spectrometer and "Tilt method" resulted in a decrease of the rates seen by electron arm, resulting in a better S/A ratio, higher hypernuclear yields, and as a result, hypernuclear spectroscopy with higher statistics and high resolution was realized.

TABLE 1. Comparison of HNSS (E89-009) [21, 22, 34, 33] and HKS (E01-011) experiment performance for ^{12}C *target.*

	E89-009	E01-011	Gain
Scattered electron momentum acceptance [MeV/c]	120	320	2.6
Solid angle of kaon arm [msr]	5	16	3.2
Kaon survival	0.37	0.34	0.94
	^{12}C target		
Beam current [μA]	0.66	22.0	33.3
Target thickness [mg/cm^2]	22	100	4.5
Virtual photon flux ($\times 10^{-6}$)	370	4.8	0.013
Singles rates of e' arm	>100 MHz	1.2 MHz	0.012
${}^{12}_{\Lambda}$B ground state doublet count	165	620	3.8
Yield rate of ${}^{12}_{\Lambda}$B ground state doublet [Hz]	$1.0{\cdot}10^{-4}$	$8.3{\cdot}10^{-4}$	8.3
S/A ratio of ${}^{12}_{\Lambda}$B ground state doublet	0.6	1.4	2.3
Width of ${}^{12}_{\Lambda}$B ground state doublet [keV]	900	465±97	

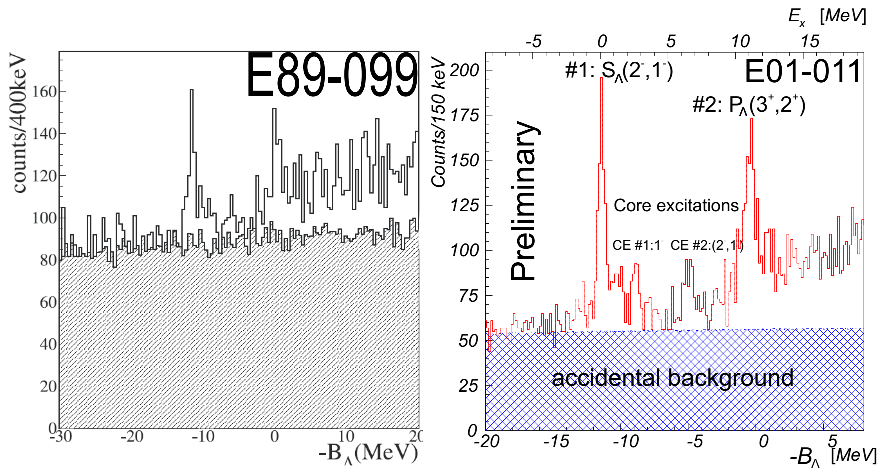

Fig. 9. Comparison between E89-099 [21] [22] and E01-011 ${}^{12}_{\Lambda}$B *spectra.*

3.1. Spectroscopy of the ${}^{12}_{\Lambda}$B *hypernucleus*

Two prominent peaks, one at $B_\Lambda \approx -11.5$ MeV and the other near the Λ emission threshold $B_\Lambda \approx 0$ MeV, are clearly evident in the spectrum, as shown in Fig. 9 and Fig. 10. They correspond to the proton-hole Λ-particle configuration, s_Λ ground state ${}^{11}\mathrm{B}(3/2^-) \otimes s_{\Lambda 1/2}$ and p_Λ substitute states ${}^{11}\mathrm{B}(3/2^-) \otimes p_{\Lambda 1/2}$ and ${}^{11}\mathrm{B}(3/2^-) \otimes p_{\Lambda 3/2}$ [35, 36]. Additionally, two peaks have been observed be-

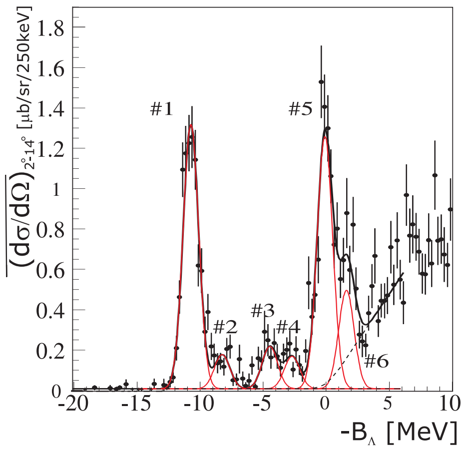

(a) KEK-E369: (π^+, K^+) reaction [42]

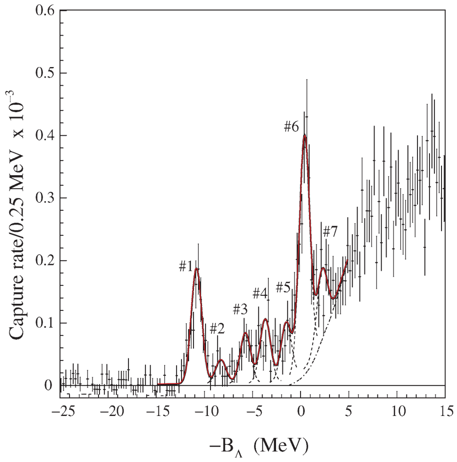

(b) INFN-DAΦNE: (π^-, K^-) [43]

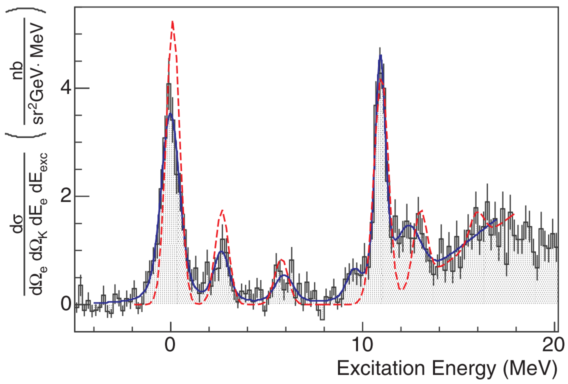

(c) JLab Hall A: E94-107 [37, 38]

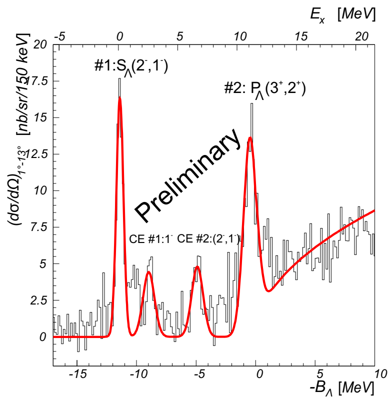

(d) Present study JLab Hall C (E01-011): $(e, e'K^+)$ reaction

Fig. 10. Hypernuclear mass spectra of ${}^{12}_{\Lambda}$C *by the (a) Exp. KEK-SKS E369:* (π^+, K^+) *reaction (b) Exp. DAΦNE-FINUDA:* (K^-, π^-) *reaction and* ${}^{12}_{\Lambda}$B *by (c) JLab Hall A : E94-107 and present study (d) JLab Hall C Exp. E01-011:* $(e, e'K^+)$ *reaction with simple four gaussian fit*

tween ground state and composite p-shell peaks. The origin of these peaks is in the coupling of the low lying ^{11}B core excited states and Λ hyperon in s-shell. The observed core excited states of $^{12}_{\Lambda}$B hypernuclei are expected to be at the same excitation energy of ^{11}B states because $^{12}_{\Lambda}$B is considered as weakly coupled ^{11}B core nucleus and Λ hyperon. The p_Λ peak, as seen from the figure, is composed of high-spin stretched states $J^\pi = 2^+$s and $J^\pi = 3^+$, with Λ remaining in the p-shell and coupled to $^{11}\mathrm{B}(\frac{3}{2}; g.s.)$ core. The importance of the $(e, e'K^+)$ reaction in the study of hypernuclei manifests here because the $J^\pi = 2^-$ in the ground state and $J^\pi = 3^+$ p-shell substitute state of the $^{12}_{\Lambda}$B can only be produced either by electroproduction or by photoproduction.

TABLE 2. Comparison of results from JLab E01-011 (Preliminary) and E92-107 [37, 38] experiments for the $^{12}_{\Lambda}$B *spectrum. Listed E01-011 excitation energy values were extracted from Gaussian response function for each of the states. Binding energy of the s-shell state is* B$_\Lambda$=*-11.40* MeV.

		Hall C E01-011		Hall A E94-107	
Peak	Structure : J$^\pi$	E_x [MeV]	FWHM$_x$ [MeV]	E_x [MeV]	FWHM$_x$ [MeV]
#1	$^{11}\mathrm{B}(\frac{3}{2}; g.s.) \otimes s_{\frac{1}{2}\Lambda} : 1^-$ $^{11}\mathrm{B}(\frac{3}{2}; g.s.) \otimes s_{\frac{1}{2}\Lambda} : 2^-$	0±0.01±0.15	0.47±0.07	0.0±0.03	1.15±0.18
CE#1	$^{11}\mathrm{B}(\frac{1}{2}; 2.12) \otimes s_{\frac{1}{2}\Lambda} : 1^-$	2.57±0.05±0.25	0.45±0.07	2.65±0.10	0.95±0.43
CE#2	$^{11}\mathrm{B}(\frac{3}{2}; 5.02) \otimes s_{\frac{1}{2}\Lambda} : 2^-$ $^{11}\mathrm{B}(\frac{3}{2}; 5.02) \otimes s_{\frac{1}{2}\Lambda} : 1^-$	6.45±0.07±0.25	0.57±0.09	5.92±0.13	1.13±0.29
#2	$^{11}\mathrm{B}(\frac{3}{2}; 5.02) \otimes s_{\frac{1}{2}\Lambda} : 2^+$ $^{11}\mathrm{B}(\frac{3}{2}; 5.02) \otimes s_{\frac{1}{2}\Lambda} : 3^+$	10.93±0.02±0.15	1.15±0.17	10.93±0.03	0.67±0.15

Hypernuclear spectrum of $^{12}_{\Lambda}$B hypernuclei obtained in the E01-011 experiment is compared to the results of two previous JLab experiments: Hall C experiment E89-009 (HNSS) [21, 22, 27, 34] (data taking in 2000) and Hall A experiment E94-107 [37, 38]. Comparison of $^{12}_{\Lambda}$B spectra from present study to HNSS result, see Fig. 9, and JLab Hall A result, see Fig. 10 (c) and (d), shows consistency of features seen as well as in the extracted central values of s-shell and p-shell state binding energies as listed in Table 2. Binding energies were calculated according to following equation:

$$-B_\Lambda = MM_{HY} - M_A - M_\Lambda \tag{2}$$

MM_{HY} is the missing mass of hypernuclei obtained with Eq. 1, M_A represents the mass of the target nucleus and M_Λ is the mass of the Λ hyperon.

Extracted binding energies of hypernuclear states were obtained by fitting each of the four prominent features of the $^{12}_{\Lambda}$B by a Gaussian of different width while the continuum spectrum in the unbound region, the so called quasifree region, was represented by the square root function. The extracted excitations from the E01-011 and E94-107 experiments are listed in Table 2. For the E01-011 experiment, excitation energy is measured with respect to the observed binding energy $B_\Lambda = -11.40$ MeV of the ground state. It should be noted that this type of fit only gives central values of each of the peaks and does not provide information on full structure of ${}^{12}_{\Lambda}$B hypernuclei. Also, because there are significant strengths around p-shell region and p-shell width itself is larger than s-shell width it is obvious that, as expected, there are multiple states in p-shell region. Further optimization of optics and analysis/simulation of response function of each of the states (with the help of theory predicted binding energies and strengths) is needed before a more precise and detailed values of binding energies can be reported.

Comparison to the mirror hypernucleus ${}^{12}_{\Lambda}$C measured by the (π^+, K^+) at KEK-SPS, measured at various time as reported in [39–42, 24] and by the (K^-, π^-) reaction at INFN-DAΦNE [43] is shown in Fig. 10. Structure of the spectra of these mirror hypernuclei shows similar characteristics with Λ s-shell and p-shell peaks clearly seen with 1.5 MeV–2 MeV resolution. Comparison of the s-shell and p-shell state's binding energies of the two mirror hypernuclei and their separation, is shown in Table 3. Data for ${}^{12}_{\Lambda}$C hypernuclei was extracted from the references [39–43, 24] Once HKS spectroscopy is finalized, the comparison of energy levels of the same spin-parity states will give valuable information about the charge-symmetry breaking effect.

TABLE 3. Comparison of experimental s-shell and p-shell binding energies and Λ s-p shell energy spacing of ${}^{12}_{\Lambda}$B and ${}^{12}_{\Lambda}$C: E336[41][24], E369[42] and [43].

Reaction	Experiment			
	-B$_\Lambda$: s-shell [MeV]	-B$_\Lambda$: p-shell [MeV]	Δsp [MeV]	$\left\{\begin{array}{l}\Delta\mathrm{sp}({}^{12}_{\Lambda}\mathrm{B})- \\ \Delta\mathrm{sp}({}^{12}_{\Lambda}\mathrm{C})\end{array}\right\}$ [MeV]
${}^{12}\mathrm{C}(e, e'K^+){}^{12}_{\Lambda}\mathrm{B}$	11.40±0.01±0.15	0.47±0.02±0.15	10.93	-
${}^{12}\mathrm{C}(\pi^+, K^+){}^{12}_{\Lambda}\mathrm{C}$ E336	10.80 (fixed)	-0.20±0.03	11.00	-0.07
${}^{12}\mathrm{C}(\pi^+, K^+){}^{12}_{\Lambda}\mathrm{C}$ E369	10.76 (fixed)	0.10±0.04	10.66	0.27
${}^{12}\mathrm{C}(K^-, \pi^-){}^{12}_{\Lambda}\mathrm{C}$	10.94±0.06	-0.27±0.06	11.21	-0.28

A preliminary spectrum of the ${}^{12}_{\Lambda}$B hypernuclei obtained with $(e, e'K^+)$ reaction at JLab Hall C and beam currents up to $30\mu A$ shows that hypernuclear spectroscopy with resolution better than 500 keV is possible. The origins of the reported systematic errors of the binding energy are due to optical calibration procedure and uncertainty of the spectrometer kinematics (beam energy and particle momenta).

3.2. Spectroscopy of the ${}^{7}_{\Lambda}$He hypernucleus

The obtained ${}^{7}_{\Lambda}$He spectrum from the ^{7}Li target is both the spectrum of the lightest neutron-rich Λ-hypenuclear system and the last information needed to complete our knowledge on the $A = 7$ hypernuclear iso-triplet ($T = 1$) system. The spectrum measured in the E01-011 experiment is shown in Fig. 11(b) and Fig. 12(b).

This hypernucleus has already been studied by emulsion experiments in 1970s but the extracted information from emulsion data on the $^7_\Lambda$He spectrum [46], as shown in Fig. 11(a), is not reliable due to insufficient statistics. The first generation hypernuclear spectroscopy experiment also studied this hypernucleus but in the HNSS spectrum, the ground state peak was not observed [22] also due to low statistics and experimental resolution (see Fig. 12(a)).

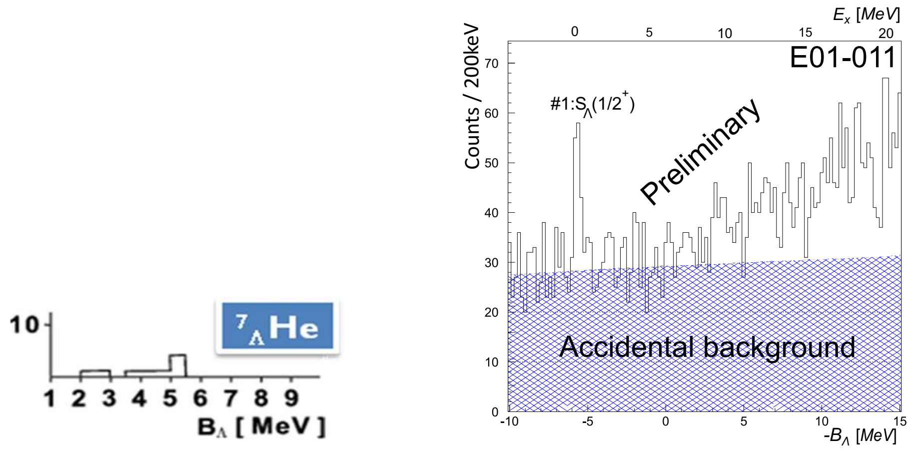

Fig. 11. Mass spectra of the $^7_\Lambda$He hypernuclei as obtained from (a) emulsion data [46] and (b) by present study, JLab Hall C Exp. E01-011: $(e, e'K^+)$ reaction

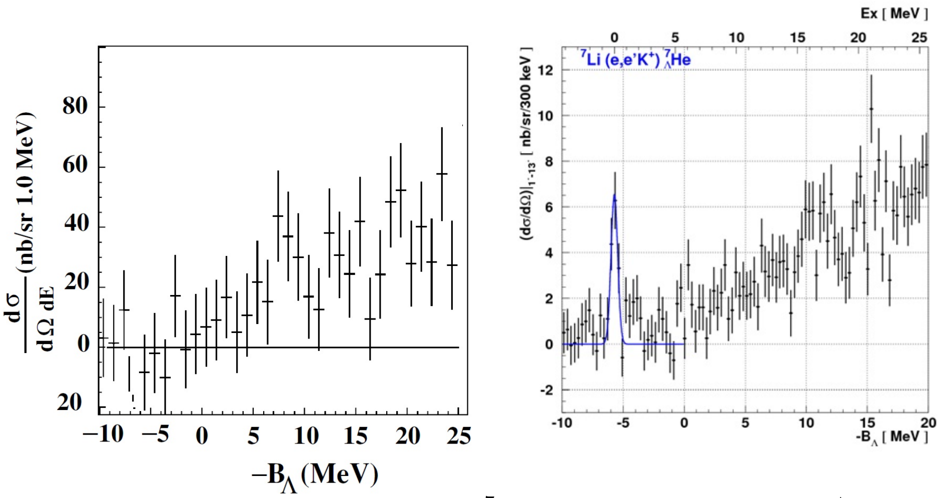

Fig. 12. The hypernuclear mass spectra of $^7_\Lambda$He hypernuclei by the $(e, e'K^+)$ reaction at JLab Hall C as obtained from (a) Exp. E89-009 (HNSS) [22] and (b) by present study: Exp. E01-011.

The present preliminary spectrum of ${}^{7}_{\Lambda}$He hypernuclei, as shown in Fig. 11(b), is the first clear evidence of the ground state $(\frac{1}{2}^+)$ peak, interpreted as being proton-hole with a Λ hyperon configuration ${}^{6}\mathrm{He}(0^+; 0.00) \otimes s_\Lambda$. Analysis of the present spectrum gives preliminary values of binding energy $B_\Lambda = 5.66 \pm 0.03(stat) \pm 0.22(sys)$ MeV (with respect to the hypernuclear threshold as defined by Eq. 2) and 520 keV width (FWHM) of the state.

3.2.1. Isotriplet A=7 hypernuclei

With the present spectrum of the neutron rich ${}^{7}_{\Lambda}$He hypernucleus and extracted (preliminary) binding energy of a Λ hyperon, full experimental results on $T = 1$ iso-triplet hypernuclei system (${}^{7}_{\Lambda}$He,${}^{7}_{\Lambda}$Li and ${}^{7}_{\Lambda}$Be) are available. Spectra of the iso-triplet members ${}^{7}_{\Lambda}$He obtained by the ${}^{7}\mathrm{Li}(e, e'K^+){}^{7}_{\Lambda}\mathrm{He}$ reaction (present study), ${}^{7}_{\Lambda}$Li obtained by the ${}^{7}\mathrm{Li}(\pi^+, K^+){}^{7}_{\Lambda}\mathrm{Li}$ reaction using SPS spectrometer at the KEK PS (experiment E336 [34, 51, 55] and ${}^{7}_{\Lambda}$Be hypernuclei obtained by the emulsion data are shown in Fig. 13.

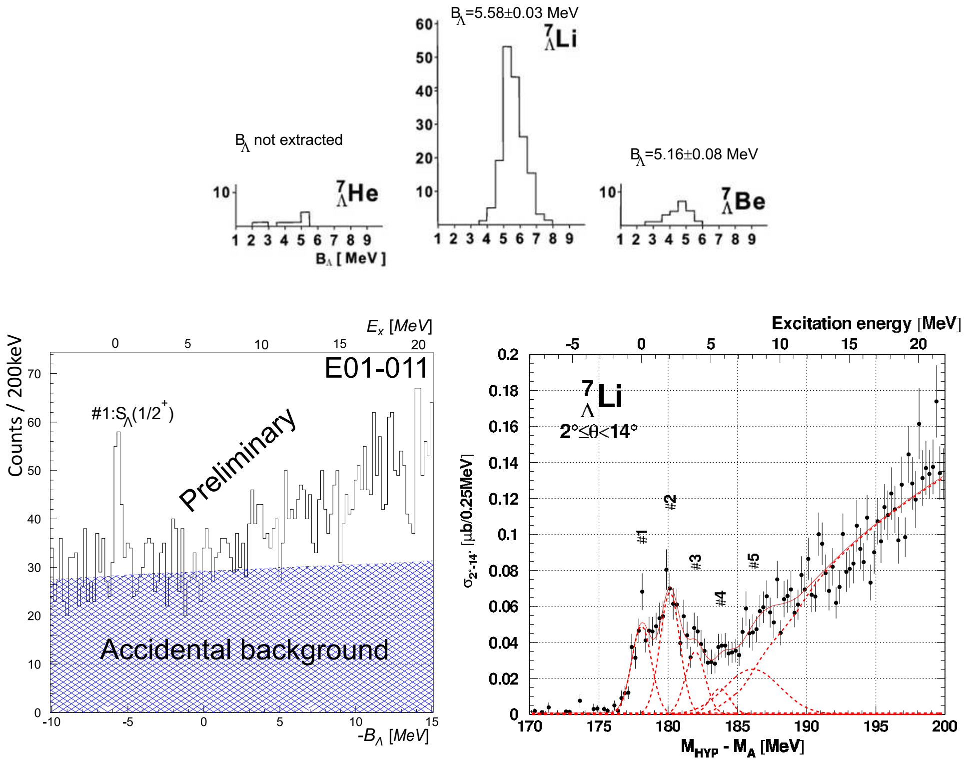

Fig. 13. The hypernuclear mass spectra of $A = 7$ isospin triplet ($T = 1$). (upper plots) emulsion data for ${}^{7}_{\Lambda}$He, ${}^{7}_{\Lambda}$Li ($T = 0$) and ${}^{7}_{\Lambda}$Be [46], (bottom left) ${}^{7}_{\Lambda}$He by present study, JLab Hall C Exp. E01-011: $(e, e'K^+)$ reaction and (bottom right) ${}^{7}_{\Lambda}$Li by the (π^+, K^+) reaction from KEK [44].

Binding energy of the $^7_\Lambda$Li, $T=1$ ground state was obtained by combining results from γ-ray spectroscopy of the $^7_\Lambda$Li hypernucleus and emulsion data of the $T=0$ $^7_\Lambda$Li hypernucleus [45]. Both results are needed because the ($T=1$, $J^\pi = \frac{1}{2}^+$) $^7_\Lambda$Li state is an excited state and decays by γ-ray emission to the ground state ($T=0$, $J^\pi = \frac{1}{2}^+$) of the $^7_\Lambda$Li hypernucleus. Mass of the $T=0$ $^7_\Lambda$Li ground state was obtained from the emulsion data [46] and mass spectrum is shown in Fig. 13(a).

With full experimental results on these $T=1$ iso-triplet hypernuclei, comparison is made with recent theoretical results of the level structures as calculated by Hiyama et al. [47] (shown in Fig. 14). Binding energy of each hypernucleus was calculated with respect to the $\alpha+\Lambda+N+N$ threshold. Thresholds of the iso-triplet hypernuclei in the core+Λ picture are also represented. Core of the $T=1$ $((1/2)^+$ $^7_\Lambda$Li is excited ($T=1$, 0^+) state of the ^{6}Li nucleus with excitation energy of 3.56 MeV with respect to the ^{6}Li ground state ($T=0$, 0^+). Theoretical calcu-

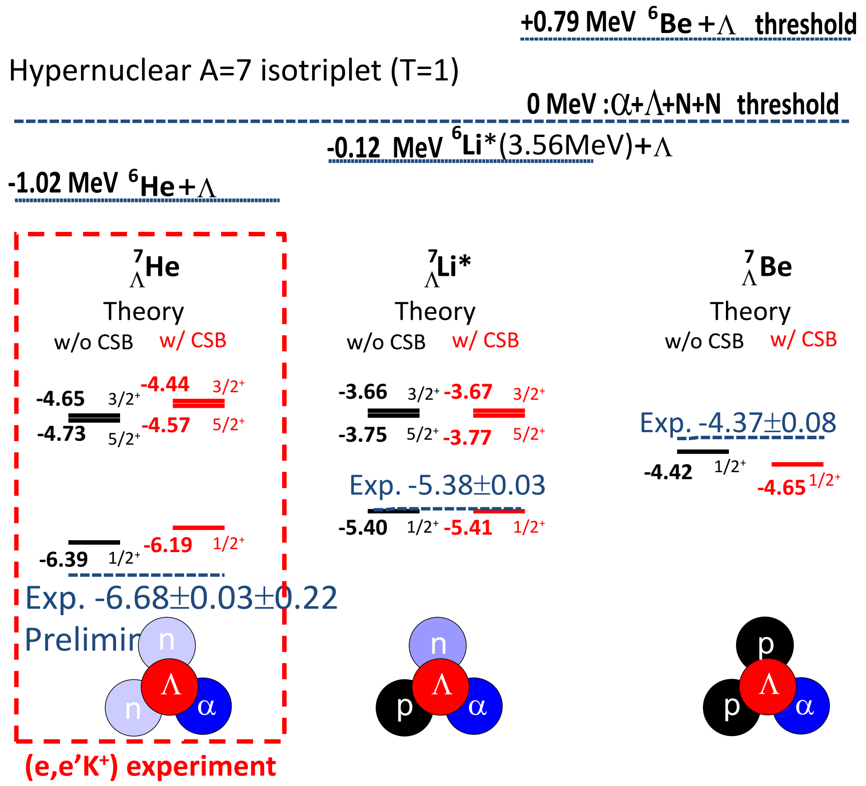

Fig. 14. Comparison of the experimental and theoretical binding energies of the A=7 isotriplet hypernuclei ($^7_\Lambda$He, $^7_\Lambda$Li and $^7_\Lambda$Be) with respect to $\alpha+\Lambda+N+N$ threshold. Energy thresholds for each of the hypernuclei (core+Λ) are also indicated.

lation was made in $\alpha + \Lambda + N + N$ four-body cluster model without charge symmetry breaking (CSB) interaction and with introduction of a phenomenological CSB interaction. Results without CSB interaction are listed in the *"w/o CSB"* column and with CSB interaction in the *"w/ CSB"* column in Fig. 14. Phenomenological CSB potential was derived [47] to explain binding energy difference of the $A = 4$ isodublet ($T = 1/2$) hypernuclei ($^4_\Lambda$H, $^4_\Lambda$He) [48–51]. With the inclusion of the CSB potential, the difference between experimental and theoretical values of the $A = 7$ hypernuclei are further increased. Further investigation of the CSB effect in other iso-multiplets of p-shell hypernuclei is needed.

3.3. *Spectroscopy of the* $^{28}_{\Lambda}$Al *hypernucleus*

The $^{28}_{\Lambda}$Al hypernuclear mass spectrum represents the first ever hypernuclear spectroscopy by the $(e, e'K^+)$ reaction with Λ populating states above the p-shell and represents a gateway toward high-mass hypernuclei. Also it is the first time ever that the $^{28}_{\Lambda}$Al hypernuclear mass spectrum has been measured. Preliminary spectrum of $^{28}_{\Lambda}$Al hypernucleus is shown in Fig. 15 together with theoretically predicted spectrum and spectrum of mirror hypernuclei $^{28}_{\Lambda}$Si.

The obtained spectrum shows two prominent peaks in the bound region and an additional peak in the unbound region. Peaks are interpreted as being proton-hole with a Λ hyperon configuration $0d^{-1}_{\frac{5}{2}} \otimes s_\Lambda$, $0d^{-1}_{\frac{5}{2}} \otimes p_\Lambda$, and $0d^{-1}_{\frac{5}{2}} \otimes d_\Lambda$, respectively. Additionally, we see significant and un-resolvable strength in between the three prominent peaks, especially between the p-shell and d-shell states, a consequence of the breakup channels of the $^{28}_{\Lambda}$Al hypernuclei. The spectrum was fitted with three Gaussians and a second-order polynomial representing the continuum part. Resolution of the observed states is better than 600keV (FWHM) and the resolution of s-shell state is 440 keV.

The mirror hypernuclei $^{28}_{\Lambda}$Si spectrum, obtained by the (π^+, K^+) reaction with SKS spectrometer at KEK and shown in Fig. 15(a), also exhibits three peaks $(\#1, \#3, \#5)$ at $B_\Lambda \approx -17 MeV$ and -8 MeV in the bound region and a broad peak at $B_\Lambda \approx 1$ MeV in the unbound region. The mentioned peaks have the same hole-particle configuration as $^{28}_{\Lambda}$Al states [52, 53] namely $0d^{-1}_{\frac{5}{2}} \otimes s_\Lambda, p_\Lambda, d_\Lambda$. The resolution of these states is 2.2, 2.7 and 6.6 MeV [54], respectively.

When comparing two mirror spectra, except significantly better (sub-MeV) resolution obtained in electroproduction spectrum, it is worth mentioning that the puzzling bump structure in the $^{28}_{\Lambda}$Si spectrum in between the s-shell and p-shell states is not evident in the preliminary $^{28}_{\Lambda}$Al results of the HKS data.

Once HKS spectroscopy is finalized, comparison of energy levels of the same spin-parity states of $^{28}_{\Lambda}$Si and $^{28}_{\Lambda}$Al hypernuclei will allow extraction of information about charge symmetry breaking (CSB) effect.

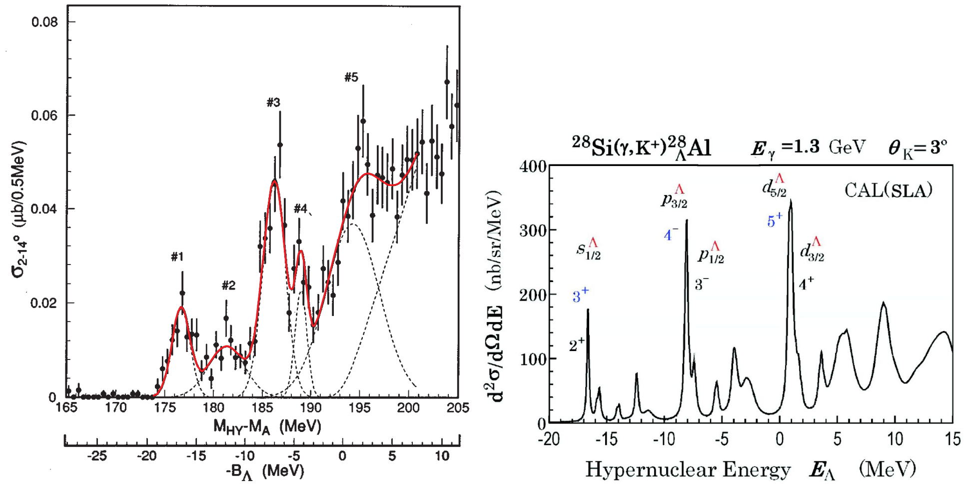

(a) KEK-E369: (π^+, K^+) reaction [40]

(b) Theoretical calculation

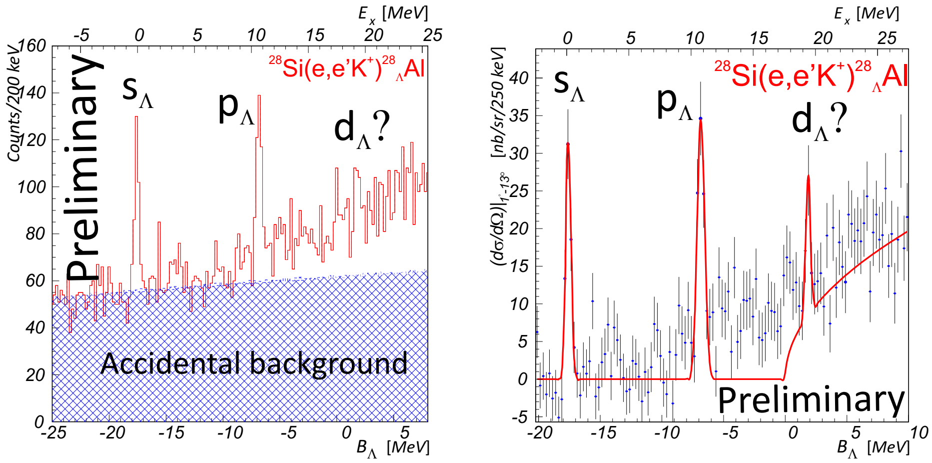

(c) Present study JLab Hall C (E01-011): $(e, e'K^+)$ reaction

Fig. 15. The hypernuclear mass spectra of (a) $^{28}_{\Lambda}$Si *by the experiment KEK-SKS E369:* (π^+, K^+) *reaction, (b) calculated spectrum for the* $^{28}\mathrm{Si}(e, e'K^+)^{28}_{\Lambda}\mathrm{Al}$ *reaction at* $E_\gamma = 1.3$ GeV *and* $\theta^{LAB}_{K^+} = 3°$ *with SLA model [55] [56] and (c)* $^{28}_{\Lambda}$Al *by present study, JLab Hall C Exp. E01-011:* $(e, e'K^+)$ *reaction*

4. *Conclusions*

In this paper successfulness of the E01-011 experiment, the 2$^{\mathrm{nd}}$ generation hypernuclear experiment at JLab Hall C, has been demonstrated with provided hypernuclear spectra of ${}^{12}_{\Lambda}$B, ${}^{7}_{\Lambda}$He and ${}^{28}_{\Lambda}$Al hypernuclei. Results from ${}^{12}_{\Lambda}$B hypernuclei confirmed possibility of high-yield, high-resolution spectroscopy with the new experimental setup.

Spectrum of ${}^{12}_{\Lambda}$B is consistent with HNSS results with much higher statistics, clear evidence of core-excited states and p-shell and width of s-shell state better than 500 keV, the best ever achieved.

With for the first time measured spectrum of ${}^{7}_{\Lambda}$He hypernucleus, information on all members (${}^{7}_{\Lambda}$He, ${}^{7}_{\Lambda}$Li and ${}^{7}_{\Lambda}$Be) of $A = 7$ hypernuclear system that forms iso-triplet $T = 1$ is now known. This will allow us to extract and discuss effects of charge symmetry breaking on the hypernuclear masses.

Spectrum of ${}^{28}_{\Lambda}$Si hypernuclei is the first ever observed hypernuclear spectrum with Λ beyond the p-shell by the $(e, e'K^+)$ reaction. This result confirmed the method for measuring spectra of medium-heavy Λ hypernuclei and as such is a gateway toward heavy (high-Z) nuclei.

Acknowledgements

These materials are based on work partly financed by the National Foundation for Science, Higher Education and Technological Development of the Republic of Croatia.

References

[1] D. H. Davis, Contemp. Phys. **27** (1986) 91.
[2] H. Bando, T. Motoba and Y. Yamamoto, Phys. Rev. C **31**, 1 (1985) 265.
[3] B. F. Gibson and E. V. Hungerford, Phys. Reports **257**, 6 (1995) 349.
[4] M. A. Faessler et al., Phys. Lett. B **46**, 3 (1973) 468.
[5] W. Bruckner et al., Phys. Lett. B **55**, 1 (1975) 107.
[6] W. Bruckner et al., Phys. Lett. B **62**, 4 (1976) 481.
[7] W. Bruckner et al., Phys. Lett. B **79**, 1–2 (1978) 157.
[8] R. E Chrien and et al., Phys. Lett. B **89**, 1 (1979) 31.
[9] R. Bertini et al., Phys. Lett. B **83**, 3–4 (1979) 306.
[10] R. Bertini et al., Nucl. Phys. A **360**, 2 (1981) 315.
[11] R. Bertini et al., Nucl. Phys. A **368**, 3 (1981) 365.
[12] A. Gal, Nucl. Phys. A **754** (2005) 91.
[13] M. Danysz et al., Nucl. Phys. **49** (1963) 121.
[14] S. Aoki et al., Prog. Theor. Phys. **85** (1991) 1287.
[15] P. H. Pile, S. Bart, R. E. Chrien et al., Phys. Rev. Lett. **66** (1991) 2585.
[16] M. Akel et al., Nucl. Phys. A **534**, 3–4 (1991) 478.
[17] A. Bamberger et al., Phys. Lett. B **36**, 4 (1971) 412.
[18] M. May et al., Phys. Rev. Lett. **53** (1983) 2085.
[19] M. May et al., Phys. Rev. Lett. **47** (1981) 1106.

[20] H. Tamura et al., Phys. Rev. Lett. **84**, 26 (2000) 5963.

[21] T. Miyoshi et al., Phys. Rev. Lett. **90**, 23 (2003) 232502.

[22] L. Yuan et al., Phys. Rev. C **73**, 4 (2006) 044607.

[23] M. Sotona, Czech. J. Phys. **50** (2000) 49.

[24] O. Hashimoto and H. Tamura, Progr. Part. Nucl. Phys. **57**, 2 (2006) 564.

[25] A. S. Rosenthal, D. Halderson, K. Hodgkinson and F. Tabakin, Annals of Phys. **184**, 1 (1988) 33–61.

[26] C. B. Dover and D. J. Millener, *Modern Topics in Electron Scattering*, World Scientific (1991) p.609, edited by B. Frois and I. Sick.

[27] O. Hashimoto et al., *Jlab E01-011 proposal: Spectroscopic study of* Λ *hypernuclei up to medium-heavy mass region through the* $(e, e'K^+)$ *reaction* (unpublished).

[28] M. Q. Tran et al., Phys. Lett. B **445**, 1–2 (1998) 20.

[29] J. Adam, J. Mares, O. Richter, M. Sotona and S. Frullani, Czech. J. Phys. **42** (1992) 1167.

[30] O. Hashimoto et al., Nucl. Phys. A **790** (2007) 679c.

[31] O. Hashimoto et al., Nucl. Phys. A **804** (2008) 125.

[32] O. Hashimoto et al., Nucl. Phys. A **835** (2010) 121.

[33] L. Yuan, *High precision hypernuclear spectroscopy study by the* $(e, e'K^+)$ *reaction*. PhD thesis, Hampton University (unpublished), 2002.

[34] T. Miyoshi, *Spectroscopic study of the* Λ *hypernuclei by the* $(e, e'K^+)$ *reaction*. PhD thesis, Tohoku University (unpublished), 2002.

[35] T. Motoba, *Mesons and Light Nuclei*, 8th Conference, edited by J. Adam et al. (2001) p.125.

[36] Toshio Motoba, Miloslav Sotona and Kazunori Itonago, Progr. Theor. Phys. Supplement **117** (1994) 123.

[37] M. Iodice et al., Phys. Rev. Lett. **99**, 5 (2007) 052501.

[38] J. J. LeRose et al., Nucl. Phys. A **804**, 1–4 (2008) 116.

[39] T. Hasegawa and et al., Phys. Rev. Lett. **74**, 2 (1995) 224.

[40] T. Hasegawa and et al., Phys. Rev. C **53** (1996) 1210.

[41] K. Itonaga, T. Motoba , O. Richter and M. Sotona Phys. Rev. C **49**, 2 (1994) 1045.

[42] T. Hotchi et al., Phys. Rev. C **64**, 4 (2001) 044302.

[43] M. Agnello et al., Phys. Lett. B **622**, 1–2 (2005) 35.

[44] O. Hashimoto et al., Nucl. Phys. A **639** (1998) 93c.

[45] H. Tamura et al., Phys. Rev. Lett. **84**, 26 (2000) 5963.

[46] M. Jurić et al., Nucl. Phys. B **52** (1973) 1.

[47] E. Hiyama, Y. Yamamoto, T. Motoba and M. Kamimura, Phys. Rev. C **80**, 5 (2009) 054321.

[48] R. H. Dalitz, R. C. Herndon and Y. C. Tang, Nucl. Phys. B **47** (1972) 109.

[49] A. R. Bodmer and et al., Phys. Rev. C **31**, 4 (1985) 1400.

[50] B. F. Gibson and D. R. Lehman, Phys. Rev. C **37**, 2 (1988) 679.

[51] Y. Akaishi, T. Harada, S. Shinmura and Khin Swe Myint, Phys. Rev. Lett. **84**, 16 (2000) 3539.

[52] P. H. Pile et al., Phys. Rev. Lett. **66**, 20 (1991) 2585.

[53] R. E. Chrien, Nucl. Phys. A **478** (1988) 705c.

[54] T. Hasegawa et al., Phys. Rev. C **53**, 3 (1996) 1210.

[55] P. Bydzovsky, M. Sotona, T. Motoba, K. Itonaga, K. Ogawa and O. Hashimoto, arXiv:0706.3836v1 [nucl-th] (2007).

[56] T.Motoba, P.Bydzovsky, M.Sotona, K.Itonaga, K.Ogawa and O.Hashimoto, *Proceedings of the 2008 Sendai International Symposium on Strangness in Nuclear and hadronic Systems*, edited by K. Maeda et al. (2008) p.184.

Λ-HIPERNUKLEARNA SPEKTROSKOPIJA VISOKOG RAZLUČIVANJA REAKCIJOM (e,e'K$^+$)

Mjerenja E01-011 (HKS) su druga generacija istraživanja u hipernuklearnoj spektroskopiji reakcijom (e,e'K$^+$) u Thomas Jefferson National Accelerator Facility (JLab). To je nastavak programa istraživanja u hipernuklearnoj fizici u JLabu Hall C započet mjerenjima E89-009 (HNSS), koja su pokazala mogućnost elektrotvorbe hiperjezgri uz razlučivanje bolje od 1 MeV. Neposredan cilj mjerenja HKS bio je proučavanje srednje teških hiperjezgri. Radi toga sagrađen je nov kaonski spektrometar (HKS) visokog različivanja i uvedena je nova metoda za označavanje raspršenih elektrona, tzv. metoda naklona (Tilt method). Opisuju se i raspravljaju prethodni spektri visokog razlučivanja hiperjezgri $^{7}_{\Lambda}$He, $^{12}_{\Lambda}$B and $^{28}_{\Lambda}$Al.